Earth and Planetary Science Letters 495 (2018) 234–241

Contents lists available at ScienceDirect

Earth and Planetary Science Letters

www.elsevier.com/locate/epsl

25 years of elevation changes of the Greenland Ice Sheet from ERS, Envisat, and CryoSat-2 radar altimetry

Louise Sandberg Sørensen [a,*], Sebastian B. Simonsen [a], René Forsberg [a], Kirill Khvorostovsky [b,d], Rakia Meister [a], Marcus E. Engdahl [c]

[a] National Space Institute, DTU Space, Geodynamics Department, Denmark
[b] Nansen Environmental and Remote Sensing Center, Norway
[c] ESA-ESRIN, EO Science, Applications and Climate Department, Italy
[d] Satellite Oceanography Laboratory, Russian State Hydrometeorological University, Saint Petersburg, Russia

ARTICLE INFO

Article history:
Received 5 May 2017
Received in revised form 30 April 2018
Accepted 7 May 2018
Available online 29 May 2018
Editor: W.B. McKinnon

Keywords:
elevation change
Greenland Ice Sheet
essential climate variable
radar altimetry

ABSTRACT

The shape of the large ice sheets responds rapidly to climate change, making the elevation changes of these ice-covered regions an essential climate variable. Consistent, long time series of these elevation changes are of great scientific value. Here, we present a newly-developed data product of 25 years of elevation changes of the Greenland Ice Sheet, derived from satellite radar altimetry. The data product is made publicly available within the Greenland Ice Sheets project as part of the ESA Climate Change Initiative programme.

Analyzing repeated elevation measurements from radar altimetry is widely used for monitoring changes of ice-covered regions. The Greenland Ice Sheet has been mapped by conventional radar altimetry since the launch of ERS-1 in 1991, which was followed by ERS-2, Envisat and currently CryoSat-2. The recently launched Sentinel-3A will provide a continuation of the radar altimetry time series. Since 2010, CryoSat-2 has for the first time measured the changes in the coastal regions of the ice sheet with radar altimetry, with its novel SAR Interferometric (SARIn) mode, which provides improved measurement over regions with steep slopes.

Here, we apply a mission-specific combination of cross-over, along-track and plane-fit elevation change algorithms to radar data from the ERS-1, ERS-2, Envisat and CryoSat-2 radar missions, resulting in 25 years of nearly continuous elevation change estimates (1992–2016) of the Greenland Ice Sheet. This analysis has been made possible through the recent reprocessing in the REAPER project, of data from the ERS-1 and ERS-2 radar missions, making them consistent with Envisat data. The 25 years of elevation changes are evaluated as 5-year running means, shifted almost continuously by one year. A clear acceleration in thinning is evident in the 5-year maps of elevation following 2003, while only small elevation changes observed in the maps from the 1990s.

1. Introduction

The Global Climate Observing System (GCOS) has defined several essential climate variables (ECVs) (Bojinski et al., 2014) to support the work of e.g. the Intergovernmental Panel of Climate Change (IPCC). As the large ice sheets respond rapidly to climate change, these have been chosen by the European Space Agency (ESA) as key areas for deriving ECVs from satellite data. 25 years (1992–2016) of elevation changes over the Greenland Ice Sheet is derived by using the recently released re-processed ERS-1 and ERS-2 radar altimetry data together with Envisat and CryoSat-2 data to support this effort.

The elevation change method is a geodetic method for determining the mass balance of a glacier or an ice sheet. This method is widely used assess the state of the ice sheets (e.g. Pritchard et al., 2009; Helm et al., 2014; Zwally et al., 2005; Sørensen et al., 2011; Shepherd et al., 2012). In Sørensen et al. (2015), an along-track method was applied to Envisat radar altimetry data and the resulting elevation change maps showed significantly improved spatial resolution due to better coverage compared to previous studies based on cross-over point analysis (Johannessen et al., 2005).

* Corresponding author.
E-mail address: slss@space.dtu.dk (L. Sandberg Sørensen).

https://doi.org/10.1016/j.epsl.2018.05.015
0012-821X/

In a previous study Levinsen et al. (2015) it was concluded that the optimal method for deriving grids of elevation changes from satellite altimeters with short repeat periods, is to combine the results obtained by cross-over and along-track analysis, giving the advantage of the higher spatial resolution from the along-track method and the lower uncertainty associated with the cross-over method. We apply such a novel combination approach to derive 5-year running mean elevation change grids from conventional radar altimetry (ERS and Envisat), covering the Greenland Ice Sheet for the period 1992 to 2011. This time series of 5-year running mean elevation changes is supplemented by two 5-year mean elevation change grids (2011–2015 and 2012–2016) derived from CryoSat-2 data. The long repeat-period of CryoSat-2 means that a plane-fit approach (Simonsen and Sørensen, 2017) is preferred over the along-track approach for deriving elevation changes.

The construction of this long time series has been made possible partly through the recent reprocessing of the ERS data set in the REAPER (Reprocessing of Altimeter Products for ERS) project (Mullard Space Science Laboratory (MSSL), U.C.L., 2014), the purpose of which was to reprocess all ERS radar altimeter data to obtain an improved, homogeneous long-term data series of elevation and elevation changes. Furthermore, in the REAPER reprocessing, the ERS datasets have been processed with the geophysical and other corrections matching the Envisat dataset, making it possible to combine the data sets from these missions.

The study presented here was carried out in the ESA Greenland Ice Sheet project within the ESA Climate Change Initiative (CCI) programme (CCI, 2016), where the overall aim is to provide reliable, long-term, satellite-based data products of Greenland Ice Sheet ECVs, which can be of use for the general public and researchers e.g. climate modelers. Within the Greenland Ice Sheet CCI, one ECV parameter is the surface elevation change (SEC). Such SEC products have now been generated through a comprehensive analysis of various algorithms and corrections to ensure a validated data product, that fulfills the defined requirements for accuracy and resolution. The combined time series of all 5-year grids provide the longest possible time span of elevation changes of the Greenland Ice Sheet in the era of remote sensing radar altimetry. This data set is e.g. a crucial input to future and ongoing studies of how to correct for changing radar penetration into the snow, and hence form the basis for future estimates of mass changes of the ice sheet.

The current paper presents in detail the elevation change data product and the methods and data that was applied to create it. Any in-depth scientific analysis of its implications is out of the scope of this paper, but will be the obvious focus of future studies and publications.

2. Data

ESA has a long history of operating radar altimeters, and to span the period from 1992 to 2016 we use data from both the European Remote Sensing (ERS) satellites (Mullard Space Science Laboratory (MSSL), U.C.L., 2014), the Environmental Satellite (Envisat) (Batoula et al., 2011), and the CryoSat-2 mission (CryoSat product handbook, 2012). The radar altimeter on ERS-1 was in operation from 1991 to 1996, ERS-2 from 1995 to 2011, Envisat from 2002 to 2012, and CryoSat was launched in 2010 and is still in operation.

In this study, we utilize Level-2 (L2) ERS-1/2 and Envisat data consisting of quality-checked, geolocated height estimates, based on the "ice-1" waveform retracker (Wingham et al., 1986). Within the REAPER project, all radar altimeter, microwave radiometer and orbit products from the ERS satellites were consistently reprocessed and aligned with the Envisat data set and format (Brockley et al., 2017). This included applying the same retrackers for all the radar data sets (Mullard Space Science Laboratory (MSSL), U.C.L., 2014; Brockley et al., 2017). We used the ice-1 dataset since the consistency within this REAPER data set was more thoroughly validated than that from the ice-2 retracker, which is why the ice-1 retracker is used here. We used several geophysical corrections to correct the height data, while the backscatter coefficient waveform parameter, Bs, is used to correct height changes, and preprocessed the data sets as described in Sørensen et al. (2015). We obtained the Envisat data directly from ESA in the form of the Level-2 Radar Altimetry Geophysical Data Record (GDR) product, and the REAPER data were provided directly by the Mullard Space Science Laboratory (MSSL). We downloaded the CryoSat-2 data from ESA in form of the recent in-depth level-2 (L2i) baseline C product.

3. Elevation change algorithms

As previously stated, we apply and combine different SEC algorithms in order to obtain an optimal SEC grid solution. These along-track, cross-over, and plane-fit methods are described in the following. The repeat-track and plane-fit methods are fundamentally solving the same equations, but we describe them as individual methods here the sake reproducibility because they do require different implementations.

3.1. Repeat-track method

When using the repeat-track method, we use all data in segments along each repeated satellite tracks to solve for both SEC and the underlying topography. The algorithm used here for deriving along-track elevation change is very similar to those presented in Sørensen et al. (2015); Flament and Rémy (2012); Sørensen et al. (2011), but it has been modified to apply to the ice-1 retracked data, which provide the user with information on the backscatter coefficient Bs, but not on waveform parameters such as the leading edge width and trailing edge slope, which were used in the Sørensen et al. (2015); Flament and Rémy (2012) studies.

The least-squares regression applied in this study is performed on all data in along-track satellite track segments with a size of 2 km:

$$\begin{aligned} H(x,y,t) = {} & H_0(\overline{x},\overline{y}) + \mathrm{d}H/\mathrm{d}t(t-\overline{t}) \\ & + dB_s(Bs-\overline{Bs}) \\ & + sx(x-\overline{x}) + sy(y-\overline{y}) \\ & + \alpha\cos(\omega t) + \beta\sin(\omega t) \\ & + \epsilon(x,y,t), \end{aligned} \tag{1}$$

where dB_s is the model parameter for the backscatter, which is included since it has been shown by Legresy et al. (2005); Legrésy et al. (2006) that the retracked height changes with the backscatter. H_0 is the mean altitude, and sx and sy describe the surface topography by its slope. The overbar indicates the mean of the measurements in a segment, $\alpha\cos(\omega t) + \beta\sin(\omega t)$ describes the seasonal signal, and ϵ is the residual between the model and the data. The segments are partly overlapping (by 50%) to increase the along-track resolution. As in Sørensen et al. (2015); Flament and Rémy (2012), a 3σ outlier rejection criteria has been applied based on the $\epsilon(x,y,t)$ values to discard individual anomalous measurements. If data from multiple missions are included in the regression, we also solve for a (temporally varying) inter-mission bias.

Due to changes in orbits within and between missions, we adopt two different approaches for obtaining repeat-track elevation changes. These are described in the following.

3.1.1. True repeat-track

We use the true repeat-track (TR) approach when working with data from a single satellite sensor, which is actively maintained in a repeat-orbit. In this case, all satellite data are indexed according to the satellite track number, i, and the along-track segment number, j, which they are associated with. The track number (or relative orbit number) is provided in the raw data files, and the segment number of a given measurement is calculated as:

$$j = \frac{\varphi_{meas} - \varphi_{min}}{N}, \tag{2}$$

where φ_{meas} is the latitude of the measurement, φ_{min} is the minimum latitude of the given data set (e.g. Greenland), and N is the resolution/segment size chosen by the user. In this study, we choose N to correspond to 2 km.

Using such indices provides a fast and efficient way of searching through and grouping data for the least squares regression in Eq. (1), and since the satellite is maintained in a repeat-orbit, no restrictions are introduced on how far away from the mean track the data are located.

3.1.2. Along-track

We use the along-track (AT) strategy when working with data from several satellite missions, or when including data from a sensor, which is not actively kept in a repeat orbit, as it was the case for Envisat after an orbit maneuver in October 2010.

Since the end-products of this procedure are along-track elevation changes, it is a demand that the majority of the data used in the least-squares regression, Eq. (1) are actually from a repeat-track campaign, which serves as the reference orbit configuration.

The data from the reference period are indexed and grouped according to 3.1.1, and the mean position $(\overline{\varphi, \lambda})$ of each (i, j) segment is determined. $(\overline{\varphi, \lambda})_{(i,j)}$ is then used as a reference point for searching through the other non-repeat datasets for close-by data. In this study, data within a distance of 2 km are collected and used together with the reference data set in a given (i, j) segment, to solve the regression in Eq. (1).

3.2. Cross-over method

The cross-over (XO) method is based on using the difference between measurements in the points of intersections of the ascending and descending satellite ground tracks. The elevation time series using XO approach are formed by applying an algorithm described in Davis and Ferguson (2004) and Khvorostovsky (2012). Time series are produced for individual grid cells of $0.2° \times 0.5°$ latitude and longitude (equivalent to approximately 20×50 km in central Greenland), and this spatial resolution was selected as a trade-off between the level of detail and the density of coverage by continuous multi-mission time series. Due to orbit changes during the operation periods for the ERS and Envisat satellites, the gaps in spatial coverage over southern and central Greenland become evident if higher resolutions are applied. We create time series from all possible combinations of average height differences, $\overline{dH}$, between three-month time intervals with one-month step yielding N time series, where N is the number of used time intervals. The individual dH differences between i and j time intervals are estimated as:

$$\overline{dH}_{i \times j} = \frac{1}{2}\left(\frac{1}{n_{A_i \times D_j}} \sum dH_{A_i \times D_j} + \frac{1}{n_{D_i \times A_j}} \sum dH_{D_i \times A_j}\right), \tag{3}$$

to account for a potential ascending/descending bias. Here, n is number of crossovers between ascending (A) and descending (D) orbits related to i and j periods respectively. This $N \times N$ matrix of $\overline{dH}$ differences is then referenced to a common time to produce the mean time series. All time intervals are used as referenced giving N mean time series to maximize the amount of data involved in the computation. From these time series, we select those consisting of the largest number of available $\overline{dH}$ values, which correspond to the same set of time intervals, and then average them to obtain the resulting time series. We form continuous time series from ERS-1, ERS-2 and Envisat data by adjusting together time series obtained separately from different satellites using the average time series for overlapping periods. Elevation time series were adjusted for variations of backscatter coefficient Bs as in Khvorostovsky (2012) to account for the changes in surface properties. The SEC trends and their standard errors are estimated from a multi-parameter linear-sinusoidal function fitted to the dH time series. We applied an iterative 3σ editing procedure was applied to the residuals between the original time series and the fitting function to discard outliers. Only time series with data points of more than 40% of the total, over considered periods, are included in the product.

3.3. Plane-fit method

The orbit of CryoSat-2 differs from ERS-1, ERS-2 and Envisat by being in a long-repeat orbit with a repeat cycle of 369 days, with a near-repeat pseudo subcycle of 30 days. This complicates the use of AT or TR. The plane-fit (PF) method proposed in Simonsen and Sørensen (2017), expands Eq. (1) to account for measurements that are not aligned in short-repeat tracks. We use data within 2 km of defined grid nodes instead of in along-track segments, and a regular grid of 1 km grid-spacing is applied. We apply a quadratic fit is applied across the area of each grid cell, rather than just the linear term used in the AT and TR methods. CryoSat-2 operates in two modes above the Greenland Ice Sheet: (1) The low-resolution mode (LRM), which is similar to conventional pulse-limited radar altimetry, and (2) the synthetic aperture radar interferometric (SARIn) mode, which applies along-track SAR processing for higher resolution, and which allows for determining the incident-angle of the radar-return echo. This mode change between the coastal and interior parts of the Greenland Ice Sheet introduces the need for also solving for a mode-bias within those grid-nodes that contain measurements from both modes. Furthermore, Simonsen and Sørensen (2017) showed that it is also necessary to solve for a bias between ascending/descending (AD) orbits, and for changes in the leading edge of the radar-echo, to account for changes in surface penetration. The full expansion is then given by

$$\begin{aligned} H(x, y, t) = {} & H_0(\bar{x}, \bar{y}) + dH/dt(t - \bar{t}) \\ & + dLeW\,(LeW - \bar{LeW}) \\ & + sx(x - \bar{x}) + sy(y - \bar{y}) + cx(x^2 - \bar{x}^2) \\ & + cy(y^2 - \bar{y}^2) + cc(x^2 - \bar{x}^2)(y^2 - \bar{y}^2) \\ & + \alpha \cos(\omega t) + \beta \sin(\omega t) \\ & + b_{AD}(-1)^{AD} + b_m(-1)^m \\ & + \epsilon(x, y, t), \end{aligned} \tag{4}$$

where cx, cy and cc are additional terms in the quadratic topography expansion, LeW is the leading edge width of the radar echo, b_{AB} is the AD-bias and AD is the logical index (0/1) describing the flight direction of the satellite, b_m is the CryoSat-2 mode-bias and m is the logical index (0/1) describing the mode (Simonsen and Sørensen, 2017). We apply an outlier editing similar to that used in the other methods.

Table 1
Time span, data sources, SEC methods, and correlation lengths used in the creation of each of the SEC grids.

Period	Mission(s)	SEC algorithm(s)	Correlation length [km]
1992–1996	ERS-1	XO	25 km
1993–1997	ERS-1/ERS-2	XO	25 km
1994–1998	ERS-1/ERS-2	XO	25 km
1995–1999	ERS1/ERS-2	XO	25 km
1996–2000	ERS-2	TR/XO	20 km
1997–2001	ERS-2	TR/XO	20 km
1998–2002	ERS-2	TR/XO	20 km
1999–2003	ERS-2/Envisat	AT/XO	20 km
2000–2004	ERS-2/Envisat	AT/XO	20 km
2001–2005	ERS-2/Envisat	AT/XO	20 km
2002–2006	ERS-2/Envisat	AT/XO	20 km
2003–2007	Envisat	TR/XO	15 km
2004–2008	Envisat	TR/XO	15 km
2005–2009	Envisat	TR/XO	15 km
2006–2010	Envisat	TR/XO	15 km
2007–2011	Envisat	AT/XO	20 km
2011–2015	CryoSat-2	PF	15 km
2012–2016	CryoSat-2	PF	15 km

4. Deriving SEC grids

We merged the SEC results from the TR, AT, and XO analyses using the method of least squares collocation (Moritz, 1980), where the error estimates from the individual elevation change results (XO, RT or AT) act as weights in the gridding to provide an optimal, combined grid estimate. The computations were done with the Gravsoft software package Tscherning et al. (1994), assuming a correlation length within the range 15–25 km, and an a priori minimum variance of 5 $cm y^{-1}$, to obtain smoothed final grid results. The a priori minimum variance is included as the basic measurement uncertainty.

Different correlation lengths are used depending on the mission and data (see Table 1). The reason for the different correlation lengths in the different solutions is that the SEC estimates based only on XO data (1992–1996 to 1996–1999) have a lower spatial resolution than those also based on repeat-track estimates. Also, in the case of mission combinations, for which the AT algorithm was implemented, and in case of the Envisat non-repeat orbit data, the spatial density is lower than in the TR results.

The post-processing gridding applied to the SEC estimates derived from CryoSat-2 data consists of interpolating onto a grid of 1 km resolution. These 1 km grid values are then filtered by applying a weighted averaging filter based on all SEC estimates within a distance of 15 km, with the weights being defined by the uncertainty of each data point and the distance to the points. This reduces the noise which otherwise dominates the elevation change results. As the true repeat of Cryosat-2 is 369 days, with a 30-days sub-cycle, a noise term is introduced by differences in the areas being observed at different seasons. This noise term is evident near coastal outlets, and is directly imprinted in the error-estimate, which again have resulted in the need for a longer correlation length applied ice sheet wide. As for ERS-1/2 and Envisat the effective spatial resolution of the product correlated is to the error map and in high-error areas it may approach the correlation length.

Table 1 summarizes the time span, data sources, SEC methods, and correlation lengths used in the SEC grid creation. The long repeat of the CryoSat-2 mission compared to the conventional radar missions means that a different gridding scheme is applied, where no a priori minimum variance is assumed.

Conventional radar altimetry struggles with mapping the margins of the Greenland Ice Sheet due to the steep slopes characterizing this area. As a consequence and to avoid extrapolation in the merged SEC grid, we exclude all grid cells which are located on slopes exceeding 1.5°, if the SEC is based on conventional radar altimetry (ERS-1, ERS-2 and Envisat). Excluding values located at higher slopes results in a ∼10% reduction of grid point values over the Greenland Ice Sheet. For a visualization of this, see Fig. 1. We interpolate data onto a 5 km grid using a circular sharp cut-off filter, and the results of the merging procedure are shown in the following section.

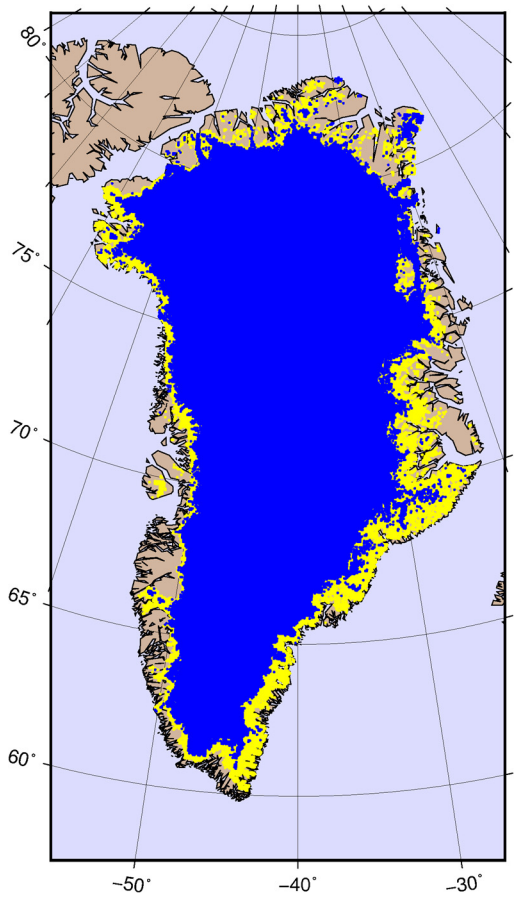

Fig. 1. Yellow indicates high-slope ice covered areas in Greenland, and blue indicates grid cells with slopes less than 1.5 degrees. Shown in yellow is the grid of the ice-covered grid cells in Greenland, and on top of this the blue grid indicates grid cells with associated surface slope less than 1.5 degrees. The blue grid covers ∼10% of the yellow grid. (For interpretation of the colors in the figure(s), the reader is referred to the web version of this article.)

For the SEC grids derived from CryoSat-2 data, we apply no data culling based on surface slope. This is due to the superior along-track resolution and geolocation made by the SARIn method resulting in a far better performance over the sloping topography characterizing the margins of the ice Sheet.

5. Results

Based on the procedures of deriving SEC estimates from the TR, AT, XO and PF methods, we have derived all possible 5-year running mean SEC grids for the periods 1992–1996 to 2012–2016. Fig. 2 (upper panel) shows five of these: 1992–1996, 1997–2001, 2002–2006, 2007–2011, and 2012–2016. Here, blue indicates ice thinning while red indicates thickening. The lower panel of Fig. 2 shows the associated error grids, with blue being minimum error and red being maximum error. As it would be expected we see that the errors increase with distance to satellite track/cross-over location where the SEC is not well constrained. The error-constrained gridding results in an effective spatial resolution, which in low-error regions approaches 5 km and in high-error areas approaching the correlation lengths listed in Table 1. The ef-

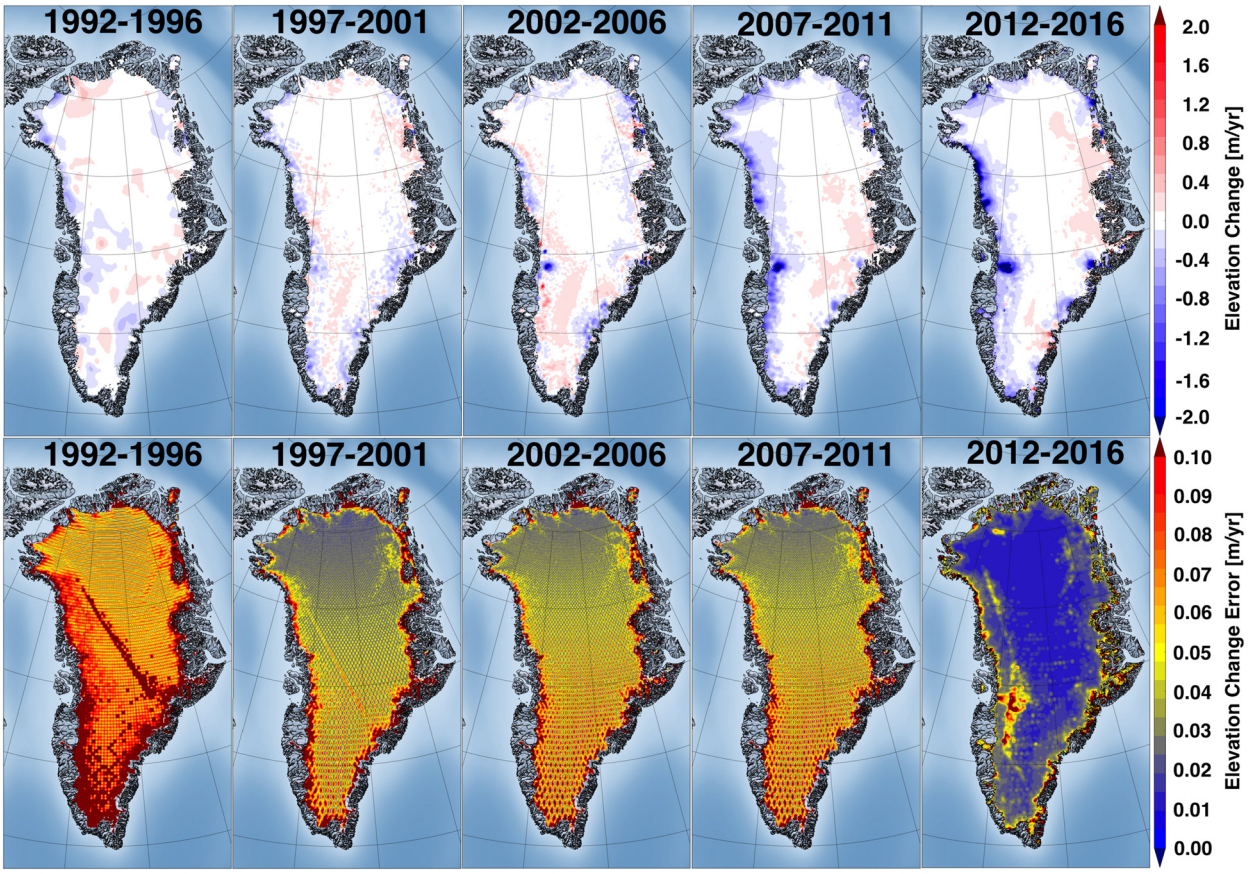

Fig. 2. The upper panel shows four elevation change grids for the Greenland Ice Sheet for the periods 1992–1996, 1997–2001, 2002–2006, 2007–2011, and 2012–2016 respectively. The lower panel shows the associated grid errors.

fective resolution is indeed 5 km in areas with high data density and quality, as seen in the error grids in the lower panel of Fig. 2.

All the 5-year SEC means and their associated errors are shown in the supplementary material. Table 1 lists which SEC algorithm and which data sets that we used for the generation of each individual SEC grid. The SEC grids for the first four periods (up until 1999) are smoother than the following ones because they are based only on XO results, and therefore have a relatively low spatial resolution. The orbit constellation for these first years of ERS data do not provide repeated data to also provide repeat-track results. Also; the error grid exhibits larger values because of the reduced number of data points used in the collocation.

We also present the accumulated volume change from a weighted sum of each SEC grid and present the accumulated volume change of the Greenland Ice Sheet and each of eight major drainage basins in the period 1992–2016 in Fig. 3. Here, the red graph represents the results when summing only the area of slope $<1.5°$, which is the coverage of the ERS and Envisat grids. The blue graph represents the results for the maximum available spatial coverage, which is largest for the CryoSat-2 results. The drainage basin delineation follows Zwally et al. (2012) and are shown in the lower left corner of Fig. 3. From Fig. 3 we see a growth of the Greenland ice sheet until approximately 2003, and that after 2003 the volume has steadily decreased to reach ≈ -1300 km^3 in 2016 when evaluating the full covered area by CryoSat-2 (the blue graph). The difference in accumulated volume change between evaluating the CryoSat SEC grids in the full CryoSat-covered area and only summing over the ERS/Envisat-covered area (surface slopes $<1.5°$) amounts to ≈ 300 km^3. A figure showing the volume changes derived from each SEC grid is provided in the Suppl. Material (Fig. S19). The different drainage basins exhibits different behavior. Basin one shows the earliest positive maximum in accumulated volume at ~2000 after which the volume decreases steadily throughout the period. The accumulated volume in basin two reaches a positive peak in ~2003 but remains rather stable hereafter. Taking the uncertainties into account, we cannot conclude that basin three has experienced a significant accumulated volume change. Basin four on the other hand is stable until ~2003, but similarly decrease hereafter. The accumulated volume changes in basins five to eight seem to reach their positive peaks in 2003–2005 after which they decrease throughout the time period. We find that basin eight contributes the most to the total accumulated volume change of the entire ice sheet.

6. Discussion

The analysis of 25 years of satellite radar altimetry data reveals significant changes in the Greenland Ice Sheet surface elevation (Fig. 2 and supporting material). The early 1990s show only areas of modest elevation changes, with no clear spatial pattern of thinning or thickening although the accumulated volume change shows a small growth until 2003 (Fig. 3). At the beginning of the new millennium a clear pattern of thinning appears and dominates a large fraction of the ice sheet margin, and individual outlet glaciers can be identified by large thinning rates, which with time propagate further onto the main ice sheet. These thinning rates exceed the errors in the associated error grids and this gives confidence that these changes are actual elevation changes and not a consequence of changes in data source, analysis or coverage.

In the 1998–2002 SEC grid, we see a clear accelerated thinning near Jakobshavn glacier, as well as along a part of the western margin, near Upernavik. A zoom on the Jakobshavn area for all

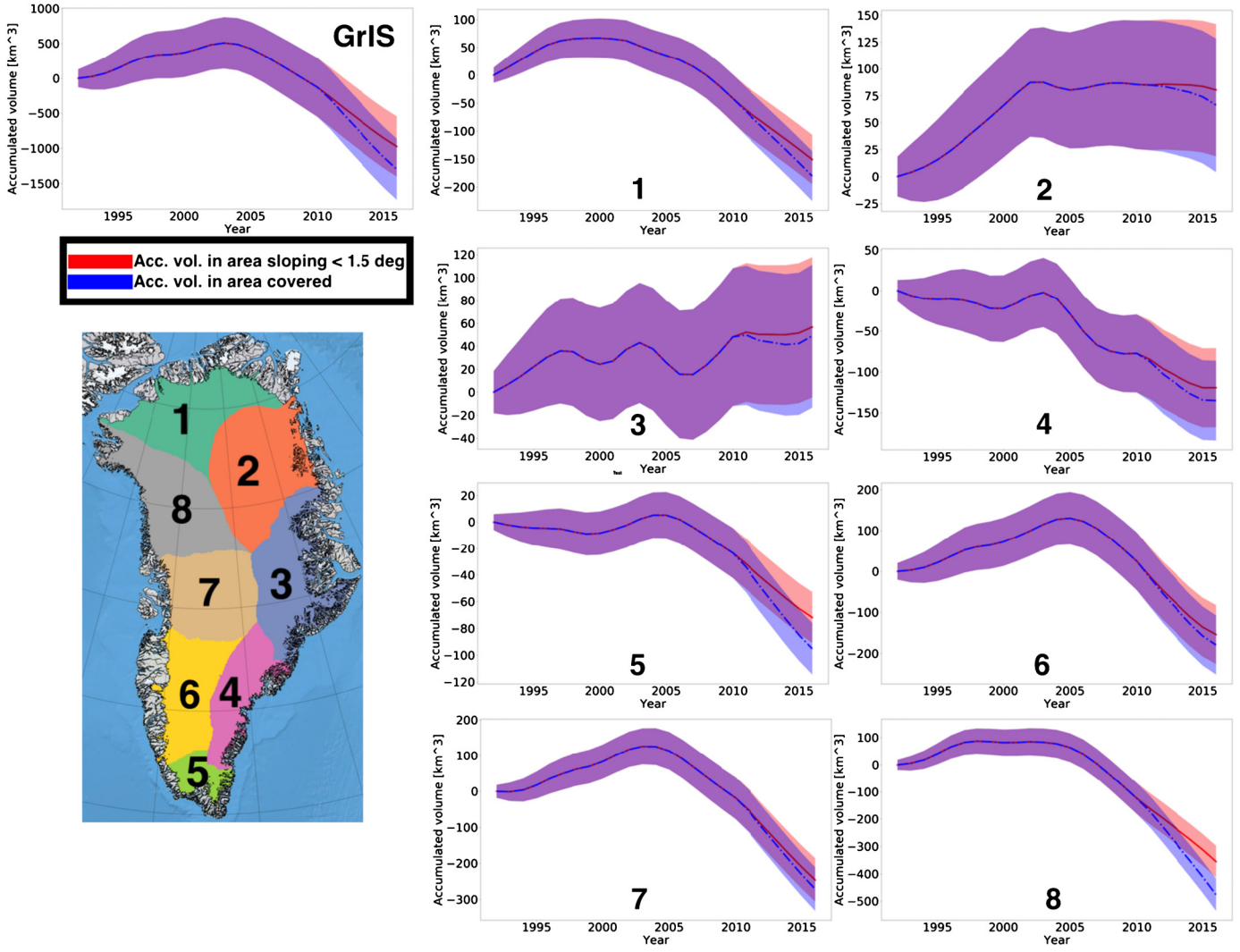

Fig. 3. Accumulated volume change of the Greenland Ice Sheet 1992–2016. The red graph shows the results for summing only the grid points of surface slope $< 1.5°$ (blue grid in Fig. 1), which are the available grid points from ERS and Envisat data. The blue graph shows the accumulated volume change when summing over the full available SEC grids, which are ∼10% larger for CS2 than for ERS and Envisat. The accumulated volume time series are shown for the entire ice sheet (GrIS) as well as for eight major drainage basins.

SEC grids are shown in the supporting material. Here we see that the thinning near Jakobshavn starts in the mid 1990s, which is almost 10 years prior to the onset of the Greenland wide volume loss in 2003. The thinning at Jakobshavn Isbræ may be linked to the loss of its larger floating ice tongue from 1998–2003 and the rapid speed-up of the Jakobshavn glacier as reported in Joughin et al. (2008).

In southeast Greenland a very clear thinning pattern appears in the 2002–2006 elevation change grid and this pattern intensifies in the 2003–2007 and 2004–2008 grids, after which it decreases. We must acknowledge that the derived grids from the conventional altimeters (ERS-1, ERS-2 and Envisat) do not cover the entire ice-covered area in Greenland, as evident in Fig. 1 due to high surface slopes in the coastal region of Greenland. This hampers a direct comparison of total volume change estimates with independent estimates from e.g. ICESat or mass changes from the GRACE mission, since in recent years the largest changes are indeed happening in these areas close to the ice margin. We see though that this issue is overcome with the results derived from CryoSat-2 data, which performs much better over topographic regions. Even though a direct comparison to independent estimates from GRACE is challenged by the possible changes in the scattering horizon of the radar altimeters and the non-trivial volume to mass conversion, we can still see that the temporal evolution of the basin-scale accumulated volume estimates (shown in Fig. 3) actually compare well in most basins with the accumulated mass changes from GRACE. We compare our accumulated volume changes with those GRACE basin time series for the Greenland ice Sheet available through the ESA Greenland Ice Sheet Climate Change Initiative, which are based on the methodology presented in Barletta et al. (2013). The GRACE time series overlap with our in the period 2002–2016 and in this period we see that basin eight is the largest contributor to both the total accumulated ice sheet volume and mass change. Also, we see some distinct similarities such as in basin two, where a negative trend is apparent in the first period (2002–2005) after which the curves flatten. For basins three and four there are discrepancies between the accumulated volume and mass changes, though. In basin three the data shows a total mass loss of ∼500 Gt, while we see no significant volume change for the same period. Also, basin four shows significantly larger mass than volume change. These discrepancies can be a consequence of e.g. increased light precipitation which has a much larger effect on the volume than mass change.

As shown by e.g. Nilsson et al. (2015) and Sørensen et al. (2015), the radar altimeters do not necessarily track the snow/air surface but penetrate into the snow. Hence, the elevation changes

derived from radar altimeters might not be the actual surface elevation changes. Under stable climate conditions, this surface penetration might actually be an advantage, as it might suppress noise induced by seasonal snowfall and give an elevation change estimate more relevant for mass balance studies than that from laser altimetry. However, the past decade has been characterized by large climate variability in Greenland, and the surface penetration is highly climate-dependent (Nilsson et al., 2015; Orsi et al., 2017). This is especially evident in the occurrence of strong melt events where the formation of ice lenses creates strong reflective surfaces for the radar altimeters (Forsberg et al., 2013; Nilsson et al., 2015). The inclusion of the backscatter coefficient in Eq. (1) when applying the TR and AT methods and using Bs for adjustment of time series derived by XO method accounts for some of this effect, but not all as shown by Simonsen and Sørensen (2017), who also showed that the LeW is an important parameter to include in the CryoSat-2 solution. This is also the reason that we include additional waveform parameters in the analysis of CryoSat-2 data, while Bs is the only waveform parameter provided along with the ice-1 retracker height estimates, which we apply in the generation of the ERS and Envisat data. Having more waveform parameters available would have been useful, as the inclusion of these could have additionally improved the SEC estimates from ERS and Envisat data. This suggests that an end-user should apply additional information from regional climate models to remove the remaining signal from changes in penetration depth to derive Greenland Ice Sheet mass balance from the SEC grids presented here. As seen in Fig. 2, the SEC grid error varies in both time and space. The overall grid error is largest in the first grids, which are based on the XO method for which the distance between SEC estimates is large compared to the AT and TR SEC estimates. Therefore, we also see a smaller error in the following SEC grids, which are based on those methods. It is also clear that the errors are generally smaller in the northern part of Greenland compared to the southern part, which is due to the much denser coverage of satellite passes towards north. As previously mentioned Fig. 3 shows that there is a significant difference in the accumulated volume change of the Greenland Ice Sheet in the years covered by CryoSat-2 data when including the regions with surface slopes of $> 1.5°$ compared to evaluating only the ERS/Envisat-covered area. This highlights that some volume change is likely to be missing in the pre-CryoSat-2 grids.

The value of deriving multi-year trends like the 5-year means presented here, compared to a product with higher temporal resolution is that high-frequency phenomena like single snowfalls or snow-redistributions are suppressed in favor of a signal that is associated with changes in mass balance. Furthermore, choosing a five-year period ensures enough data to derive robust SEC estimates even after discarding outliers.

The methodologies used in this study have been validated thoroughly in previous studies (Khvorostovsky, 2012; Simonsen and Sørensen, 2017; Levinsen et al., 2015). We apply the methodologies on a reprocessed and improved data set for ERS-1/2 and combine the various data sets, which makes it possible to create the 25-year time series. We refer to the extensive validation carried out in those previous studies, but note that unfortunately no or very little data exist to validate the SEC grids in the period covered by ERS-1 and ERS-2. The instruments and orbits of the ERS satellites are similar though to the Envisat data, which is validated by Operation IceBridge airborne data (Levinsen et al., 2015).

7. Conclusion

We present 25 years of elevation changes over the Greenland Ice Sheet derived from radar altimetry from the ERS-1, ERS-2, Envisat and CryoSat-2 missions. We have applied both repeat-track, cross-over, and plane-fit methods to derive 5-year mean SEC estimates, and these are merged and interpolated onto a 5 km grid using collocation to cover $\approx 90\%$ of the ice sheet for the ERS-1/2 and Envisat data, and the entire ice sheet for the CryoSat-2 data. The difference in ice coverage is a result of the poor performance of conventional radar altimetry over highly variable topography, which is overcome by the SARIn mode of CryoSat-2 mission.

These grids of SEC and their associated errors are publicly available for download through the ESA Greenland Ice Sheet CCI website (http://www.esa-icesheets-greenland-cci.org/).

We find that in the earlier years of this 20-year time series no distinct thinning or thickening pattern is evident, but that in the later years thinning is observed along most of the ice sheet margin. We also observed that the temporal onset of this thinning is variable, with the thinning of the Jakobshavn glacier being one of the first thinning areas.

Over the full time period drainage basin eight in western Greenland contributed the most to the full ice sheet accumulated volume change, and we find that generally, the basins in West-, North- and South-Greenland have experienced large volume losses compared to the ones in East Greenland.

Acknowledgements

We thank the European Space Agency Climate Change Initiative (ESA CCI) for supporting the analysis through the Ice_Sheets_CCI project (Greenland) 2012–18. The project was funded via ESA-ESRIN contract number 4000104815/11/I-NB.

Appendix A. Supplementary material

Supplementary material related to this article can be found online at https://doi.org/10.1016/j.epsl.2018.05.015.

References

Barletta, V.R., Sørensen, L.S., Forsberg, R., 2013. Scatter of mass changes estimates at basin scale for Greenland and Antarctica. Cryosphere 7, 1411–1432.

Batoula, S., Urien, S., Soulat, F., Muir, A., Roca, M., Cotton, D., 2011. Envisat altimetry level 2 user manual, Issue 1.4.

Bojinski, S., Verstraete, M., Peterson, T.C., Richter, C., Simmons, A., Zemp, M., 2014. The concept of essential climate variables in support of climate research, applications, and policy. Bull. Am. Meteorol. Soc. 95, 1431–1443.

Brockley, D.J., Baker, S., Féménias, P., Martínez, B., Massmann, F.-H., Otten, M., Paul, F., Picard, B., Prandi, P., Roca, M., et al., 2017. REAPER: reprocessing 12 years of ERS-1 and ERS-2 altimeters and microwave radiometer data. IEEE Trans. Geosci. Remote Sens. 55, 5506–5514.

CryoSat Product Handbook, 2012. ESA, UCL. https://earth.esa.int/documents/10174/125272/CryoSat_Product_Handbook.

Davis, C.H., Ferguson, A.C., 2004. Elevation change of the Antarctic ice sheet, 1995–2000, from ERS-2 satellite radar altimetry. IEEE Trans. Geosci. Remote Sens. 42, 2437–2445.

ESA Ice Sheets Climate Change Initiative, 2016. http://www.esa-icesheets-cci.org (Accessed 15 March 2016).

Flament, T., Rémy, F., 2012. Dynamic thinning of Antarctic glaciers from along-track repeat radar altimetry. J. Glaciol. 58, 830–840.

Forsberg, R., Sandberg Sørensen, L., Levinsen, J.F., Nilsson, J., 2013. Mass loss of Greenland from GRACE, ICESat and CryoSat. In: Proceedings of CryoSat Workshop. Dresden 2013. In: ESA Special Publication, vol. 717, paper S6-4.

Helm, V., Humbert, A., Miller, H., 2014. Elevation and elevation change of Greenland and Antarctica derived from CryoSat-2. Cryosphere 8, 1539–1559.

Johannessen, O.M., Khvorostovsky, K., Miles, M.W., Bobylev, L.P., 2005. Recent ice-sheet growth in the interior of Greenland. Science 310, 1013–1016.

Joughin, I., Howat, I.M., Fahnestock, M., Smith, B., Krabill, W., Alley, R.B., Stern, H., Truffer, M., 2008. Continued evolution of Jakobshavn Isbrae following its rapid speedup. J. Geophys. Res., Earth Surf. 113.

Khvorostovsky, K.S., 2012. Merging and analysis of elevation time series over Greenland ice sheet from satellite radar altimetry. IEEE Trans. Geosci. Remote Sens. 50, 23–36.

Legresy, B., Papa, F., Remy, F., Vinay, G., van den Bosch, M., Zanife, O.-Z., 2005. ENVISAT radar altimeter measurements over continental surfaces and ice caps using the ICE-2 retracking algorithm. Remote Sens. Environ. 95, 150–163.

Legrésy, B., Rémy, F., Blarel, F., 2006. Along track repeat altimetry for ice sheets and continental surface studies. In: Proceedings of the Symposium on 15 years of Progress in Radar Altimetry. Venice, Italy, 13–18 March 2006. ESA-SP614, Paper volume 181.

Levinsen, J.F., Khvorostovsky, K., Ticconi, F., Shepherd, A., Forsberg, R., Sørensen, L.S., Muir, A., Pie, N., Felikson, D., Flament, T., et al., 2015. ESA ice sheet CCI: derivation of the optimal method for surface elevation change detection of the Greenland ice sheet – round robin results. Int. J. Remote Sens. 36, 551–573.

Moritz, H., 1980. Advanced Physical Geodesy, 1st ed. Herbert Wichmann Verlag, Karlsruhe.

Mullard Space Science Laboratory (MSSL), U.C.L., 2014. REAPER – Product handbook for ERS Altimetry reprocessed products, Issue 3.1. URL: https://earth.esa.int/documents/10174/1511090/Reaper-Product-Handbook-3.1.pdf.

Nilsson, J., Vallelonga, P., Simonsen, S.B., Sørensen, L.S., Forsberg, R., Dahl-Jensen, D., Hirabayashi, M., Goto-Azuma, K., Hvidberg, C.S., Kjær, H.A., et al., 2015. Greenland 2012 melt event effects on CryoSat-2 radar altimetry. Geophys. Res. Lett. 42, 3919–3926.

Orsi, A.J., Kawamura, K., Masson-Delmotte, V., Fettweis, X., Box, J.E., Dahl-Jensen, D., Clow, G.D., Landais, A., Severinghaus, J.P., 2017. The recent warming trend in North Greenland. Geophys. Res. Lett. 44 (12), 6235–6243. https://doi.org/10.1002/2016GL072212.

Pritchard, H.D., Arthern, R.J., Vaughan, D.G., Edwards, L.A., 2009. Extensive dynamic thinning on the margins of the Greenland and Antarctic ice sheets. Nature 461, 971–975. https://doi.org/10.1038/nature08471.

Shepherd, A., Ivins, E.R., Geruo, A., Barletta, V.R., Bentley, M.J., Bettadpur, S., Briggs, K.H., Bromwich, D.H., Forsberg, R., Galin, N., et al., 2012. A reconciled estimate of ice-sheet mass balance. Science 338, 1183–1189.

Simonsen, S.B., Sørensen, L.S., 2017. Implications of changing scattering properties on Greenland ice sheet volume change from CryoSat-2 altimetry. Remote Sens. Environ. 190, 207–216.

Sørensen, L., Simonsen, S., Nielsen, K., Lucas-Picher, P., Spada, G., Adalgeirsdottir, G., Forsberg, R., Hvidberg, C., 2011. Mass balance of the Greenland ice sheet (2003–2008) from ICESat data – the impact of interpolation, sampling and firn density. Cryosphere 5 (1), 173–186.

Sørensen, L.S., Simonsen, S.B., Meister, R., Forsberg, R., Levinsen, J.F., Flament, T., 2015. Envisat-derived elevation changes of the Greenland ice sheet, and a comparison with ICESat results in the accumulation area. Remote Sens. Environ. 160, 56–62.

Tscherning, C., Knudsen, P., Forsberg, R., 1994. Description of the GRAVSOFT Package. Geophysical Institute, University of Copenhagen. Technical Report.

Wingham, D., Rapley, C., Griffiths, H., 1986. New techniques in satellite altimeter tracking systems. In: Proceedings of IGARSS'86 Symposium, Ref. ESA SP-254, pp. 1339–1344.

Zwally, H.J., Giovinetto, M.B., Beckley, M.A., Saba, J.L., 2012. Antarctic and Greenland Drainage Systems. (Accessed 2017-12-01).

Zwally, H.J., Giovinetto, M.B., Li, J., Cornejo, H.G., Beckley, M.A., Brenner, A.C., Saba, J.L., Yi, D., 2005. Mass changes of the Greenland and Antarctic ice sheets and shelves and contributions to sea-level rise: 1992–2002. J. Glaciol. 51, 509–527.